JOURNAL OF GUIDANCE, CONTROL, AND DYNAMICS
Vol. 29, No. 5, September–October 2006

# Effect of Piezoelectric Hysteresis on Helicopter Vibration Control Using Trailing-Edge Flaps

S. R. Viswamurthy* and Ranjan Ganguli†
*Indian Institute of Science, Bangalore 560 012, India*

DOI: 10.2514/1.17655

**This study investigates the effect of piezoelectric actuator hysteresis on helicopter vibration control using trailing-edge flaps. An aeroelastic analysis is used represent the helicopter with trailing-edge flaps. A compressible unsteady aerodynamic model is used to predict the incremental airloads due to trailing-edge flap motion. The material and mechanical hysteresis in the piezoelectric actuator is modeled using the classical Preisach model. Experimental data from the literature are used to estimate the weighting function through geometric interpretation and numerical implementation. Results are obtained from vibration control studies performed using a trailing-edge flap with 1) ideal linear actuator and 2) real actuator with hysteresis modeled. Multicyclic control input gives 90 and 81% reduction in hub vibration at high-speed flight ($\mu = 0.30$) for the ideal and real actuator, respectively. In low-speed flight ($\mu = 0.15$), the hub vibration is reduced by 99 and 86% for ideal and real actuator, respectively. Results indicate that the presence of actuator hysteresis nonlinearity leads to deterioration in controller performance and lower vibration reductions in both high- and low-speed forward flight.**

## Nomenclature

| | | |
|---|---|---|
| $C_T$ | = | rotor thrust coefficient |
| $c$ | = | blade chord |
| $c_f$ | = | trailing-edge flap chord |
| $d_0$ | = | drag coefficient |
| $\mathrm{EI}_y$ | = | flap bending stiffness |
| $\mathrm{EI}_z$ | = | lag bending stiffness |
| $F_x$ | = | hub longitudinal shear force |
| $F_y$ | = | hub lateral shear force |
| $F_z$ | = | hub vertical shear force |
| GJ | = | torsion stiffness |
| $J$ | = | objective function |
| $M_x$ | = | hub roll moment |
| $M_y$ | = | hub pitch moment |
| $M_z$ | = | hub yaw moment |
| $m_f$ | = | trailing-edge flap mass per unit length |
| $m_0$ | = | blade mass per unit length |
| $N$ | = | number of control input harmonic |
| $N_b$ | = | number of blades |
| $R$ | = | rotor radius |
| $\mathbf{T}$ | = | transfer matrix of control sensitivities |
| $u$ | = | input to the hysteresis transducer/voltage applied to the piezostack, V |
| $\mathbf{u}$ | = | vector of control input harmonics |
| $\mathbf{W_u}$ | = | weighting matrix on control input |
| $\mathbf{W_Z}$ | = | weighting matrix on vibration magnitudes |
| $X_g^f$ | = | trailing-edge flap center of gravity (after hinge) |
| $\mathbf{Z}$ | = | vector of 4/rev hub loads |
| $\Omega$ | = | rotor angular speed |
| $\delta$ | = | output of the hysteresis transducer/flap deflection angle, deg |
| $\gamma$ | = | lock number |
| $\mu$ | = | advance ratio/weighting function of the hysteresis transducer |
| $\sigma$ | = | blade solidity ratio |
| $\psi$ | = | blade azimuth angle |

*Subscripts*

| | | |
|---|---|---|
| $i$ | = | control step number |
| Nc | = | $N$th cosine harmonic |
| Ns | = | $N$th sine harmonic |
| St | = | steady component |
| 0 | = | parameter evaluated at baseline conditions |

*Superscript*

| | | |
|---|---|---|
| $4p$ | = | 4/rev component |

## Introduction and Objectives

HELICOPTERS suffer from severe vibration levels compared with fixed-wing aircrafts. Helicopters have a very high degree of aeroelastic interaction because the flexibility of the rotor blades couples strongly with the aerodynamics and dynamics. The main source of vibration in a helicopter is the main rotor which operates in a highly unsteady aerodynamic environment. Severe vibration levels in a helicopter lead to passenger and crew discomfort, decreased fatigue life of structural components, and increased maintenance costs. Passive vibration isolators and absorbers are normally used to reduce vibration but they lead to considerable weight penalty and perform poorly under off-design conditions. In comparison, active vibration control systems can adapt to various flight conditions and, in general, incur lesser weight penalty. Most active vibration control systems in rotorcraft are designed to cancel the vibratory loads before they reach the airframe. Higher harmonic control (HHC) is one such active method in which the swashplate is excited at the higher harmonics of the rotor rotational speed, thereby generating new unsteady airloads that cancel the hub vibratory loads [1,2]. However, HHC suffers from certain drawbacks: 1) high actuation power, 2) large weight penalty due to hydraulic actuators, 3) limitation of excitation frequency to integer multiples of $N_b$/rev, and 4) additional airworthiness considerations.

Individual blade control (IBC) is a well-known active vibration control methodology among rotorcraft engineers and can be implemented in several ways in a helicopter. In the conventional IBC approach, the entire blade is oscillated in the pitch direction at its root using servo-actuators [3,4]. The drawbacks of this conventional IBC

Presented as Paper 2247 at the 46th AIAA/ASME/ASCE/AHS/ASC Structures, Structural Dynamics and Materials Conference, Austin, Texas, 18–21 April 2005; received 12 May 2005; revision received 13 February 2006; accepted for publication 16 February 2006. 

*Research Student, Department of Aerospace Engineering; murthy@aero.iisc.ernet.in.

†Associate Professor, Department of Aerospace Engineering; ganguli@aero.iisc.ernet.in. Senior Member AIAA.

approach are high actuation power and high pitch link loads. Both HHC and conventional IBC systems actuate the blades at the root, and therefore require higher actuation power. Another implementation of IBC involves twisting the entire rotor blade by actuating embedded or surface-mounted piezoelectric materials [5]. On-blade partial span trailing-edge flaps can be actuated at higher harmonics of the rotor rotational speed to generate new unsteady airloads, which when phased properly can lead to considerable suppression in hub vibration [6]. The actively controlled flap (ACF) approach can be implemented in single or dual flap configurations. Each flap is individually controlled in the rotating frame. This method has received considerable attention due to its simplicity of implementation and enhanced airworthiness, because the flap control is independent of the primary control system. Furthermore, the power consumed by the trailing-edge flap system for vibration suppression is much lesser compared with the conventional IBC approach [3]. Another advantage of the ACF approach is the possibility of attaching servo-flaps to helicopter rotor blades in current use with minimal redesign costs.

The ACF approach has been tested on scaled rotors in the wind tunnel [7,8]. A recent study has concluded that the ACF concept has the potential to satisfy the general requirements for primary flight controls in a helicopter with a torsionally soft rotor [9]. Besides model scale rotor tests, several studies have looked at aeroelastic analysis of a helicopter rotor with trailing-edge flaps. Milgram et al presented a comprehensive study of vibration reduction in helicopters using an actively controlled trailing-edge flap [10,11]. The aeroelastic analysis in their study included a nonlinear aeroelastic rotor model, unsteady compressible aerodynamics of the flap, and a multicyclic flap controller. The analytical results presented in their study were validated using experimental wind tunnel data. They also conducted a parametric study for a four-bladed Sikorsky S-76 main rotor. Straub and Charles investigated the dynamics and aerodynamics of rotors with trailing-edge flaps using two different aeroelastic codes [12].

De Terlizzi and Friedmann combined the rational function approximation (RFA) approach with a free-wake model to determine the aerodynamic loads under attached flow conditions [13]. In a recent study, Liu et al. developed a coupled aeroelastic and aeroacoustic simulation of a helicopter and validated it with experimental data [14]. Using a dual flap configuration, they were able to simultaneously reduce blade-vortex-interaction-induced vibration and noise at low-speed descent flight. A comprehensive review of the work on trailing-edge flaps for helicopter vibration reduction is given by Friedmann [15]. In other studies, trailing-edge flaps have been proposed for primary control of swashplateless rotors and stabilization of helicopter following damage to pitch links [16,17]. Zhang et al. looked at active-passive vibration reduction using trailing-edge flaps and optimal blade structural properties [18]. These studies do not address the effect of piezoceramic hysteresis on the trailing-edge flap control even though piezoceramic stack actuators are the leading contenders for trailing-edge flap actuation. Spencer et al. studied the possibility of employing an adaptive neurocontroller to suppress vibration using a piezoactuated trailing-edge flap [19]. The controllers employ a single hidden layer neural network, learning in real time, to adaptively cancel the effects of periodic aerodynamic loads on the blades. This neurocontroller learns the transfer function between the hub loads and the piezoceramic voltage input in real time and is therefore capable of handling piezoceramic hysteresis.

Smart materials such as piezoceramics have great potential for use in helicopters. They are light, compact, possess high bandwidth, and consume less power. Among the various methods explored to actuate the flap, piezostack actuators used in conjunction with an amplification mechanism show good promise for full-scale rotor applications. Lee and Chopra successfully demonstrated the performance of this actuation device in conjunction with a double-lever (L-L) amplification mechanism through tests in an open-jet wind tunnel [20]. In another study, Hall and Prechtl developed a discrete trailing-edge servo-flap actuator called an *X*-frame actuator and successfully conducted tests on a $1/6$ Mach scaled model rotor system to demonstrate the actuator control authority [21].

Piezoceramic materials exhibit significant nonlinear behavior at high field strengths such as voltage dependent nonlinearities (increase or decrease of electromechanical coupling coefficients) as well as hysteresis. Hysteresis in piezoceramic materials is a form of nonlinearity with memory. Thus, the piezoceramic expansion depends not only on the current voltage excitation but also on the history of excitation. This material nonlinearity couples with the amplification mechanism to yield significant nonlinearity at the structural level. Unmodeled hysteresis in the actuator can lead to inaccuracy in open-loop control and generate amplitude-dependent phase shifts, leading to poor performance of the active trailing-edge flap mechanism. Most studies related to active control of helicopter vibration using smart materials neglect the presence of material and mechanical hysteresis and nonlinearity. In a rare study addressing hysteresis effects, Kurdila et al. derived a control methodology that accounts for overall hysteresis in PZT actuated on-blade elevons [22]. However, they represented the helicopter by a very simple linear aeroelastic model and the objective was not active vibration control. They used a simple collocated output velocity feedback to study the stability of the aeroelastic system. They found that the introduction of actuator hysteresis led to a sharp degradation in the performance of collocated feedback control, sometimes even leading to loss of asymptotic stability. In the current work, the effect of piezoelectric and mechanical hysteresis nonlinearity on helicopter vibration control using trailing-edge flap is studied under high- and low-speed flight regimes. The material and mechanical hysteresis in the piezoelectric actuator is modeled using the classical Preisach model. This nonlinear actuator model is cascaded with the nonlinear aeroelastic model.

## Aeroelastic Analysis

A nonlinear model of four elastic rotor blades dynamically coupled to a 6-degree-of-freedom rigid fuselage represents the helicopter. Each blade undergoes flap bending, lag bending, elastic twist, and axial displacement. Small strains and finite rotations (moderate deflections) are assumed and the Euler–Bernoulli hypothesis is used. The trailing-edge flaps are assumed to be an integral part of the blade. The trailing-edge flap hinge is assumed to coincide with its leading edge. The flap hinges are assumed to be rigid in all directions except about the hinge axis, thereby allowing only pure rotation of the flap in the plane of the blade cross section. It is also assumed that the flaps do not contribute to the stiffness of the rotor blade and influence the behavior of the blade only through their contribution to the blade spanwise aerodynamic and inertial loading.

The aerodynamic forces and moments acting on the blade section are calculated for unsteady profile and flap motion under forward flight condition. The attached flow formulation is based on the indicial response method in which response is calculated from a finite difference approximation to the Duhamel's integral. Compressibility effects are implicitly included in the indicial response functions [23]. A time domain unsteady aerodynamic model developed by Hariharan and Leishman for a flapped airfoil in compressible, subsonic flow is used [24]. The formulation is based on linearization of the governing partial differential equations similar to that applied in classical thin airfoil theory. The present analysis considers the incremental effects on flap and profile aerodynamics caused by trailing-edge flap motions. The wake behind the rotor disk determines the induced inflow distribution over the disk and plays an important role in the prediction of the blade response, blade loads, acoustic signature, and rotor performance. The results in the present study are based on the Leishman–Bagai free-wake model [25]. The aerodynamic model in this study does not include a dynamic stall model.

The aeroelastic formulation is based on a generalized Hamilton's principle applicable to nonconservative systems:

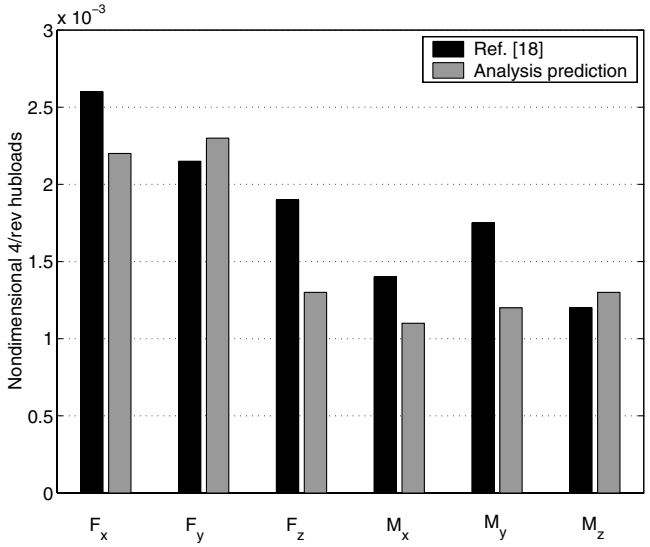


**Fig. 1 Comparison of baseline hubload prediction with aeroelastic analysis given in [18].**

$$\int_{\psi_1}^{\psi_2} (\delta U - \delta T - \delta W)\, \mathrm{d}\psi = 0 \tag{1}$$

The $\delta U$, $\delta T$, and $\delta W$ are the virtual strain energy, kinetic energy, and work, respectively. Finite element methodology is used to discretize the governing equations of motion and allows for nonuniform blade properties. The beam is discretized into 10 finite elements and each of these 10 beam finite elements have 15 degrees of freedom. The spatial functionality is removed by using finite element discretization and partial differential equations are converted to ordinary differential equations.

To reduce the computational cost, the finite element equations in terms of the nodal displacements are transformed into modal space. Four flap, four lag, and two torsion modes are used in this study. The blade response is solved in modal space using finite element in time. Eight time elements are used and fifth-order Lagrange polynomials are used as shape functions. A coupled trim/aeroelastic solution procedure is carried out to simultaneously solve for blade nonlinear steady response, pilot input trim controls, and vehicle orientation. Steady and vibratory components of the rotating frame blade loads are calculated using force summation method. In this approach, blade inertia and aerodynamic forces are integrated directly over the length of the blade. Fixed frame hub loads are calculated by summing the contributions of individual blades at the root. The hub forces and moments are nondimensionalized with respect to $m_0\Omega^2R^2$ and $m_0\Omega^2R^3$, respectively. Additional details of the aeroelastic analysis are given in [26]. Figure 1 shows the comparison of the baseline vibration levels ($\mu = 0.30$) predicted by the aeroelastic analysis used in the current study with the analysis given by Zhang et al. [18]. The vibration levels shown are for a four-bladed rotor whose properties are given in the same reference. Zhang et al. used a quasi-steady aerodynamic model to predict the aerodynamic loads acting on the rotor blades. In the current study, an unsteady aerodynamic model proposed by Leishman is used [27]. Furthermore, the free-wake model is implemented differently in the two studies [25,28]. This explains the difference in the vibration levels predicted in the two studies. Accurate prediction of hubloads is a difficult problem in rotorcraft, and aeroelastic codes generally give different predictions due to differences in modeling. However, the trends predicted by the analyses are similar and are quite useful for rotor response prediction and controller design [12]. Note that the global controller used in this study can be fine-tuned using flight-test data [2].

## Actuator Hysteresis Model

A major limitation of piezoceramic actuators is their lack of accuracy due to hysteresis and drift. Piezoceramic materials are fundamentally nonlinear in their response to an applied electric field, exhibiting a hysteresis effect between the electric field and the displacement. Mechanical linkages designed to amplify the stroke of piezoceramic actuators further amplify this hysteresis effect. In addition, there can be other sources of nonlinear behavior, such as binding or friction in the actuator mechanism, or nonlinear gain. Not modeling hysteresis in the piezoceramic actuator can lead to inaccuracy in open-loop control and generate amplitude-dependent phase shifts. Modeling and prediction of hysteresis is therefore critical for the performance of the active trailing-edge flap mechanism.

Researchers have studied hysteresis in ferromagnetic materials for long. The most popular hysteresis model for ferromagnetic materials is the classical Preisach model [29]. There exists considerable similarity between the primary hysteresis mechanism of ferromagnetic and ferroelectric materials. Several researchers have successfully applied the classical Preisach model to represent hysteresis in ferroelectric material systems. Sreeram and Naganathan were the first to apply the classical Preisach model to piezoceramic material systems [30]. Hughes and Wen discussed and verified the applicability of Preisach model to piezoceramic and shape memory alloy systems [31]. The parameter identification based on the input/output data and hysteresis compensation via direct inversion of the identified model was also demonstrated. Ge and Jouaneh used a modified Preisach model to represent hysteresis in a stacked piezoceramic actuator and validated the model through experiments [32].

Krasnoselskii separated Preisach's model from its physical meaning and represented it in a pure mathematical form [33]. As a result, this model can now be used for the mathematical description of hysteresis of any physical nature. The Preisach model has several appealing features including its ability to model complex hysteresis types, a well defined identification algorithm, and a convenient numerical simulation form [34]. The classical Preisach model can be represented in the following mathematical form:

$$\delta(\psi) = \iint_{\alpha \geq \beta} \mu(\alpha, \beta)\hat{\gamma}_{\alpha\beta}[u(\psi)]\, \mathrm{d}\alpha\, \mathrm{d}\beta \tag{2}$$

where $\hat{\gamma}_{\alpha\beta}$ is the elemental hysteresis operator. The output of each elemental hysteresis operator traces a rectangular loop on the input-output diagram switching from $-1$ to $+1$ when the input increases above the threshold $\alpha$. The output switches from $+1$ to $-1$ when the input decreases below the value of $\beta$ as shown in Fig. 2. The weighting function, $\mu(\alpha, \beta)$ is characteristic of the hysteresis transducer (Fig. 3). If the weighting function is known, then Eq. (2) can be solved directly by integration. If the function $\mu(\alpha, \beta)$ is not

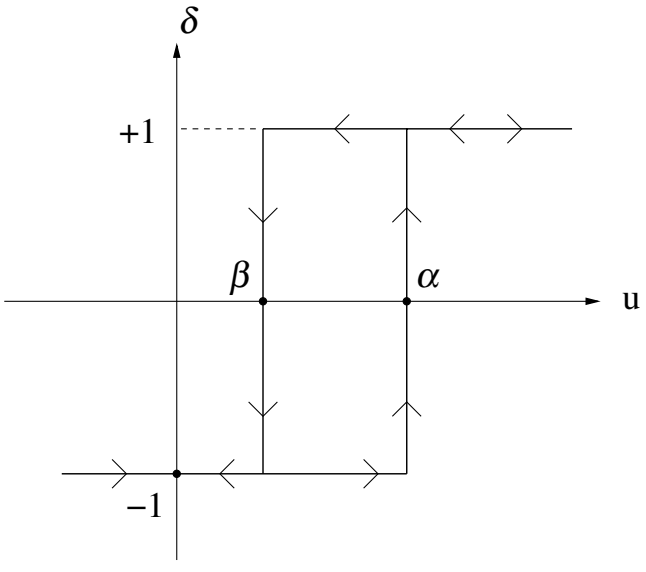


**Fig. 2 Elementary hysteresis operator.**

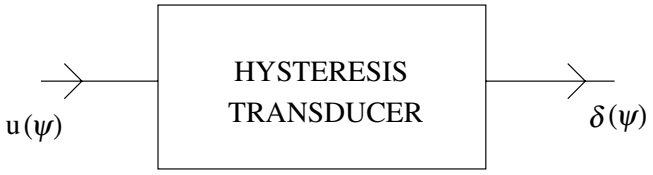


**Fig. 3 Schematic representation of a hysteresis transducer system.**

known explicitly, then experimental data are needed to estimate the weighting function through the geometric interpretation and numerical implementation [34]. In the current study, the experimental data obtained by Hall and Prechtl were used to estimate the weighting function [21].

Another important requirement for the numerical implementation of the classical Preisach model is the knowledge of the initial state of the hysteresis transducer. The initial state of the transducer along with the initial input to the transducer determines the initial output. The following output values obviously depend on the initial output value. In this study, it is assumed that the initial output of the system either corresponds to the value on the limiting ascending branch (when initial input rate is positive) or the limiting descending branch (when initial input rate is negative). Such an assumption allows us to easily fix the initial state of the hysteresis transducer.

## Control Algorithm

In the current study, a single active trailing-edge flap located at 70% blade span location is used to introduce control input directly in the rotating reference frame (Fig. 4). In steady forward flight, the helicopter rotor system can be assumed to be periodic in time. This periodic nature of the system allows us to transform the control problem from the time domain to the frequency domain [35]. The control algorithm is based on the minimization of an objective function that is a quadratic function of hub vibratory loads and control input magnitudes. In this study, the control input is the voltage applied to the piezostack and not the flap deflection angle itself.

For a four-bladed rotor, the voltage input to the piezostack is typically 3, 4, or 5/rev or a combination of all the preceding harmonics to reduce the vibratory hub loads. In the current study, a dc bias is also given to the piezostack. This dc bias is adjusted so as to obtain a flap motion with zero steady component. The total voltage applied to the piezostack is then given by Eq. (3).

$$u(\psi) = u_{\mathrm{St}} + \sum_{N=3}^{5}[u_{\mathrm{Nc}}\cos(N\psi) + u_{\mathrm{Ns}}\sin(N\psi)] \tag{3}$$

At the $i$-th control step, the objective function for optimal control is given by

$$J(\mathbf{Z}_i, \mathbf{u}_i) = \mathbf{Z}_i^T\mathbf{W}_Z\mathbf{Z}_i + \mathbf{u}_i^T\mathbf{W}_u\mathbf{u}_i \tag{4}$$

where

$$\mathbf{Z}_i = \left[F_x^{4p}F_y^{4p}F_z^{4p}M_x^{4p}M_y^{4p}M_z^{4p}\right]^T$$
$$\mathbf{u}_i = \left[u_{3c}u_{3s}u_{4c}u_{4s}u_{5c}u_{5s}\right]^T \tag{5}$$

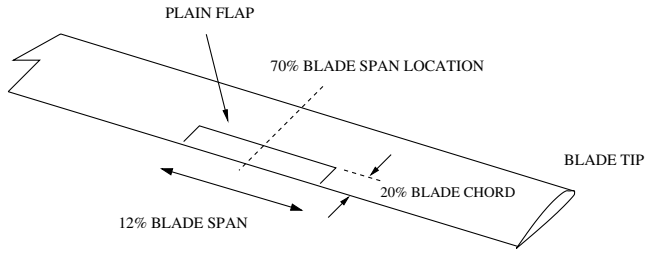


**Fig. 4 Schematic view of the rotor blade with trailing-edge flap.**

The subscript $i$ in Eqs. (4) and (5) refers to the $i$th control step, reflecting the discrete-time nature of the control. The time interval between each control step must be sufficient to allow the system to return to the steady state so that the vibration level can be measured accurately. A linear, quasi-static, frequency domain representation of helicopter response to control input is generally used in the minimization of the objective function [3]. Because $u_{\mathrm{St}}$ is not an independent parameter, it is not included in the vector of control input harmonics $\mathbf{u}_i$.

In this study, the "feedback form of the global controller" is implemented because the system is only moderately nonlinear [36,37]. This controller is a compromise between the global and the local controller. The feedback form of the global controller can save computation time without losing accuracy for a moderately nonlinear system. The transfer matrix is assumed to be constant over the entire range of control inputs just like in the global controller. However, this controller is a closed-loop form where the control input during each control step is determined by feedback of the measured vibration levels of the previous control step. Linearizing the system about the current control inputs using Taylor series expansion gives

$$\mathbf{Z}_i = \mathbf{Z}_{i-1} + \mathbf{T}_0(\mathbf{u}_i - \mathbf{u}_{i-1}) \tag{6}$$

$\mathbf{T}_0$ is the transfer matrix which is numerically computed by perturbing the control harmonics about the zero values and using a finite difference method. Equation (6) is substituted in Eq. (4) and the following optimality criteria in applied:

$$\frac{\partial J}{\partial \mathbf{u}_i} = 0 \tag{7}$$

The optimal controller then becomes

$$\mathbf{u}_i^* = \mathbf{C}_0\mathbf{Z}_{i-1} - \mathbf{C}_0\mathbf{T}_0\mathbf{u}_{i-1} \qquad \mathbf{C}_0 = -\mathbf{D}_0\mathbf{T}_0^T\mathbf{W}_Z$$
$$\mathbf{D}_0 = (\mathbf{T}_0^T\mathbf{W}_Z\mathbf{T}_0 + \mathbf{W}_u)^{-1} \tag{8}$$

## Numerical Results

Numerical results are obtained for a four-bladed, soft inplane, uniform hingeless rotor similar to the BO105 rotor. The baseline helicopter blade and trailing-edge flap properties are shown in Table 1. Studies are conducted at both high- ($\mu = 0.30$) and low-speed ($\mu = 0.15$) flight conditions. The primary source of vibration in these two flight conditions are different. In high-speed flight, the main source of vibration is the increased magnitude and periodicity of the aerodynamic loads. In low-speed flight, the rotor wake remains close to the blades and results in higher wake induced loading.

To obtain a realistic model of hysteresis, experimental data from the published literature are used. Figure 5 shows the quasi-static

**Table 1 Baseline blade and flap properties**

| Blade properties | |
|---|---|
| $N_b$ | 4 |
| $c$/R | 0.055 |
| Solidity, $\sigma$ | 0.07 |
| Lock number, $\gamma$ | 5.20 |
| $C_T/\sigma$ | 0.07 |
| Blade pretwist | 0.0 |
| Precone, $\beta_p$ | 0.0 |
| $\mathrm{EI}_y/m_0\Omega^2R^4$ | 0.0108 |
| $\mathrm{EI}_z/m_0\Omega^2R^4$ | 0.0268 |
| $\mathrm{GJ}/m_0\Omega^2R^4$ | 0.00615 |
| $m_0$, kg/m | 6.46 |
| $\Omega$, rpm | 383 |
| $R$, m | 4.94 |
| Trailing-edge flap properties | |
| $c_f/c$ | 0.20 |
| $m_f/m_0$ | 0.10 |
| $X_g^f/c_f$ | 0.20 |

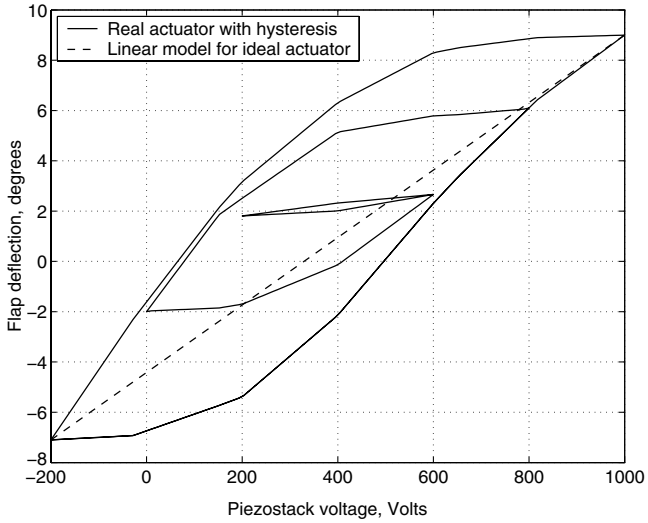


**Fig. 5 Trailing-edge flap actuator hysteresis from Hall and Prechtl [21] and the linear approximation.**

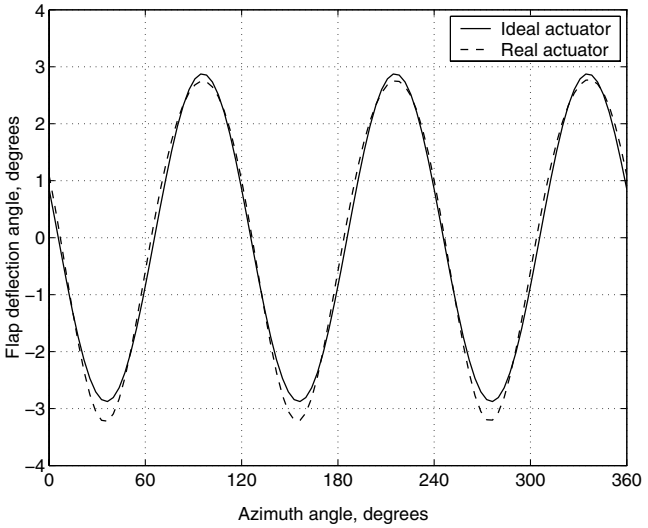


**Fig. 7 Flap motion history due to 3/rev control input, $\mu = 0.30$.**

response of a trailing-edge flap actuator on a bench top test obtained by Hall and Prechtl [21]. The hysteresis nonlinearity is due to both material effects and friction in the mechanical device. The stacks used in this research were made of lead magnesium niobate-lead titanate (PMN-PT) composition. The experimental data shown in Fig. 5 are used to determine the unknown weighting function $\mu(\alpha, \beta)$ required by the Preisach model in Eq. (2). If the entire flap actuation mechanism is assumed to have no hysteresis, then it is reasonable to presume that the relationship between piezostack voltage input and flap deflection angle is linear. This presumed linear relationship is also shown in Fig. 5. When a pure sinusoidal voltage input is given to such a linear actuator with no hysteresis, the output (flap deflection) is also a pure sinusoid with zero phase shift and at the same frequency. However, a sinusoidal input given to an actuator with hysteretic behavior yields an output (flap deflection) which has a phase shift at the input frequency and a nonzero response at other frequencies.

Two cases are considered:

Case 1) Ideal linear actuator

Case 2) Real actuator, hysteresis addressed using Preisach model

The linear actuator is termed ideal because hysteresis that occurs in the real actuator leads to an unwanted nonlinearity which complicates the controller design and adversely affects performance. The helicopter aeroelastic model is found to be almost linear with respect to the actuator control input. Hence, for the ideal linear actuator, the global controller is used to determine the optimal control input. For the real actuator with hysteresis, the feedback form of the global controller is used to determine the optimal control input, because the inclusion of the actuator hysteresis model made the overall system nonlinear. Initial studies are conducted by applying the higher harmonics of the control input individually (3, 4, and 5/rev). This provides a general understanding of the influence of the control input on the various components of the fixed-frame hub vibratory loads.

### Vibration Reduction at High-Speed Flight ($\mu = 0.30$)

3/rev *Voltage Input*

Figure 6 shows the time history of the optimal 3/rev control input (voltage input to the piezostack) for the two cases. There is a notable difference in magnitude and phase of the optimal control input obtained for the ideal and real actuator. It can be seen that the flap motion history is almost identical for the ideal and real actuator, though the 3/rev control input required to achieve this flap motion is different in the two cases (Fig. 7). In other words, the controller is able to adjust the control input for the real actuator to obtain a flap motion similar to the ideal actuator. Figure 8 shows the flap deflection angle as a function of piezostack voltage for the two cases.

Overall vibration reduction of 79% is obtained in both the ideal and real actuators. For the ideal actuator, longitudinal and lateral hub shear are reduced by about 28% each. However, the vertical shear is reduced by about 86%. The rolling, pitching, and yawing moments

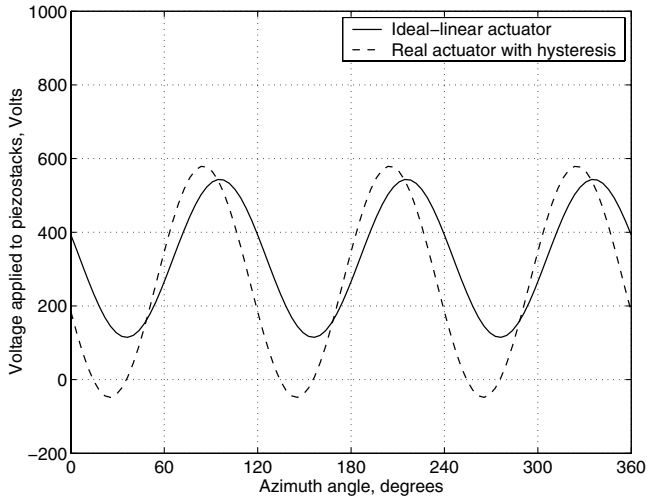


**Fig. 6 Optimal 3/rev control input, $\mu = 0.30$.**

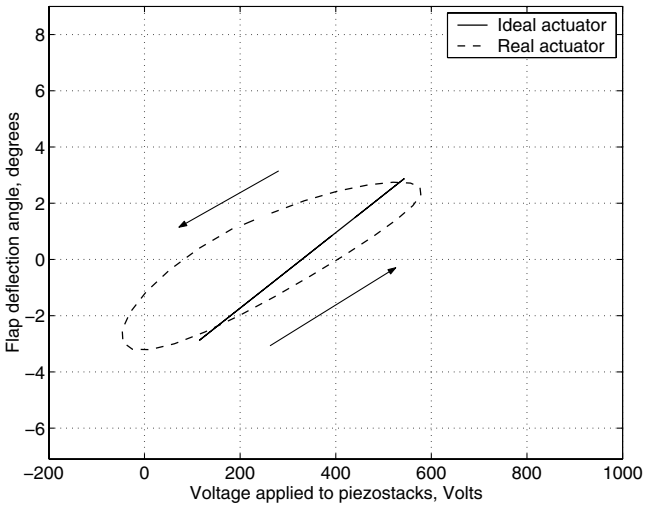


**Fig. 8 Flap motion history vs piezostack voltage for 3/rev control input, $\mu = 0.30$.**

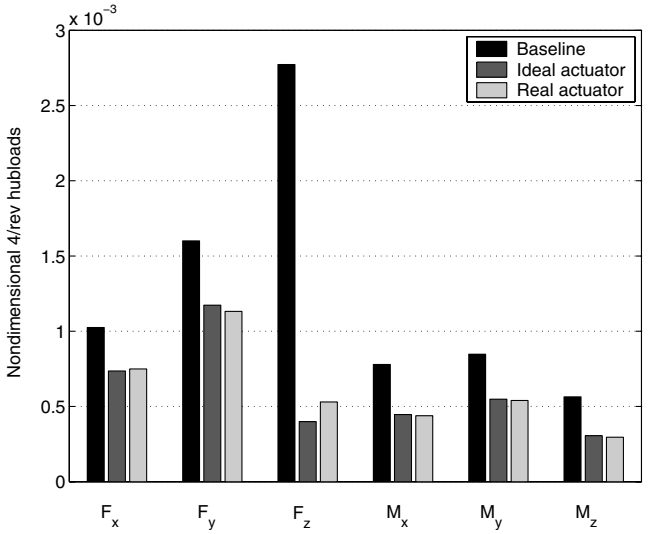


**Fig. 9 Comparison of hub vibratory loads for 3/rev control input, $\mu = 0.30$.**

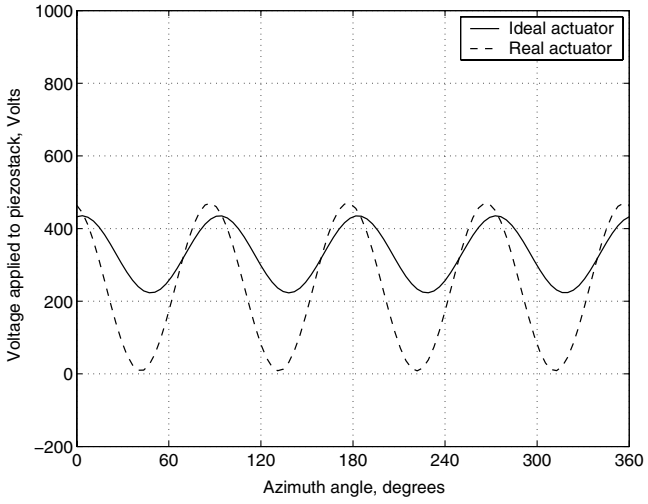


**Fig. 10 Optimal 4/rev control input, $\mu = 0.30$.**

are reduced by 43, 35, and 46%, respectively. Similar reductions in hubloads are achieved for the real actuator (see Fig. 9). The identical performance of the two cases is not surprising because the optimal flap motion achieved in both cases are nearly same.

### 4/rev *Voltage Input*

Figure 10 shows the time history of the optimal 4/rev control input for the two cases. Again, there is a notable difference in magnitude and phase of the optimal 4/rev control input obtained for the ideal and real actuator. The resulting flap motion in both cases are again found to be identical. Overall vibration reduction of 70% is obtained in both cases. For the ideal actuator, longitudinal and lateral hub shear are reduced by about 15% each (see Fig. 11). However, the vertical shear is reduced by about 92%. The rolling, pitching, and yawing moments are reduced by 15, 9, and 25%, respectively. Similar reductions in hubloads are achieved for the real actuator.

### 5/rev *Voltage Input*

Figure 12 shows the optimal 5/rev control input for the ideal and real actuators. The resulting flap motion in both cases are identical, just as seen with 3/rev and 4/rev control input. The 5/rev control input required to achieve this identical flap motion is different in the two cases. We notice that if the actuator response is modeled fairly

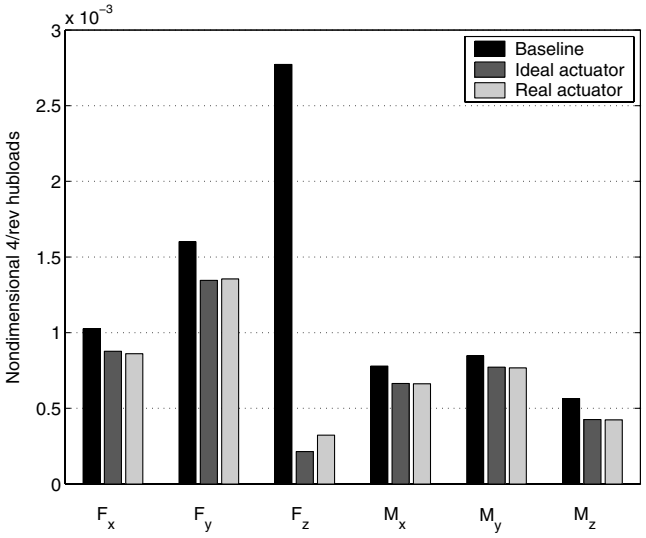


**Fig. 11 Comparison of hub vibratory loads for 4/rev control input, $\mu = 0.30$.**

well, the controller is able to adjust the magnitude and phase of the control input so as to get the precise optimal motion of the trailing-edge flap to obtain maximum vibration reduction. Overall vibration reduction of 66% is obtained for both the ideal and real actuators. For the ideal actuator, the longitudinal and vertical hub shear forces are reduced by 41 and 96%, respectively. However, the lateral shear force increased marginally by about 2%. Both pitching and yawing moments are reduced by about 24%. The rolling moment increased by 5% from the baseline value. Similar reductions in hubloads are achieved for the real actuator (see Fig. 13).

In all the three cases with individual 3, 4, and 5/rev voltage control input, the flap motion obtained using the feedback form of global controller for a real actuator has nearly the same magnitude and phasing as the flap motion obtained using the global controller for an ideal linear actuator. This is the reason why similar reduction in hub vibratory loads were obtained for the ideal and real actuator using a single frequency control input. This is because, for the real actuator, the system response is only mildly nonlinear with respect to individual voltage control inputs. Hence, the feedback form of global controller used in this study works quite well.

### *Multicyclic Control Input*

A multicyclic control algorithm is used where 3, 4, and 5/rev harmonics of the control input are given simultaneously [Eq. (3)].

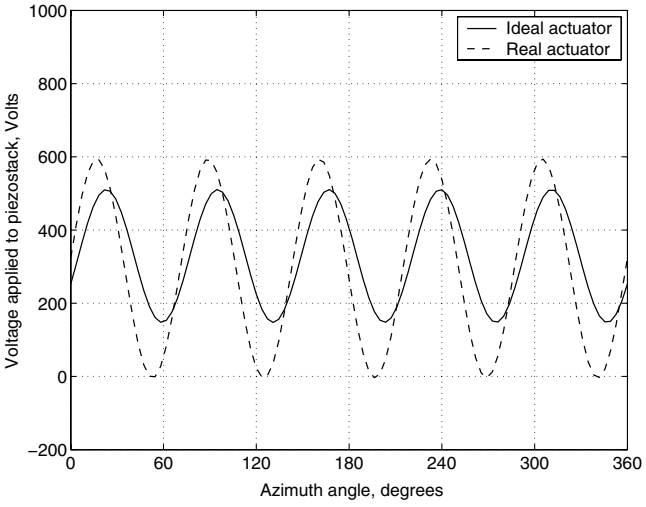


**Fig. 12 Optimal 5/rev control input, $\mu = 0.30$.**

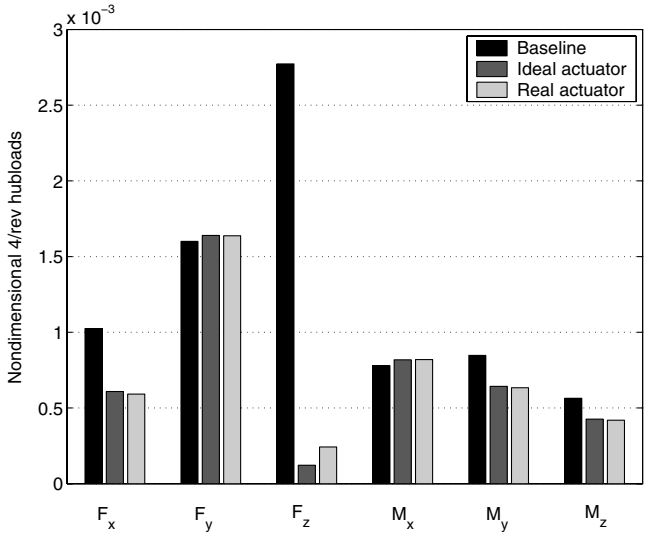


**Fig. 13 Comparison of hub vibratory loads for 5/rev control input, $\mu = 0.30$.**

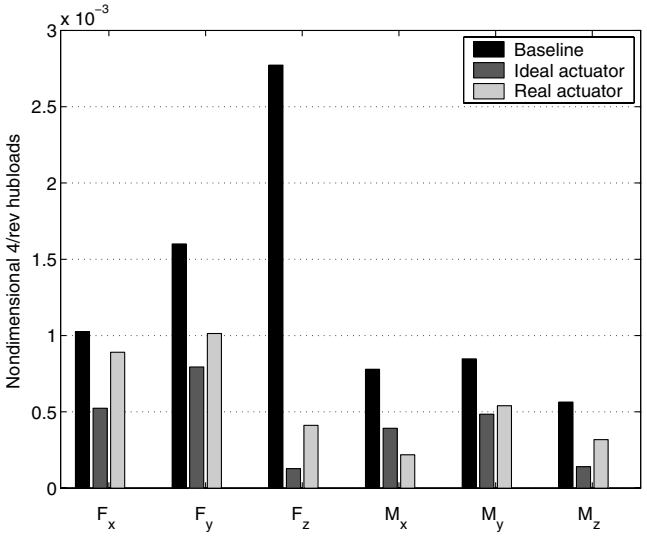


**Fig. 16 Comparison of hub vibratory loads for multicyclic control input, $\mu = 0.30$.**

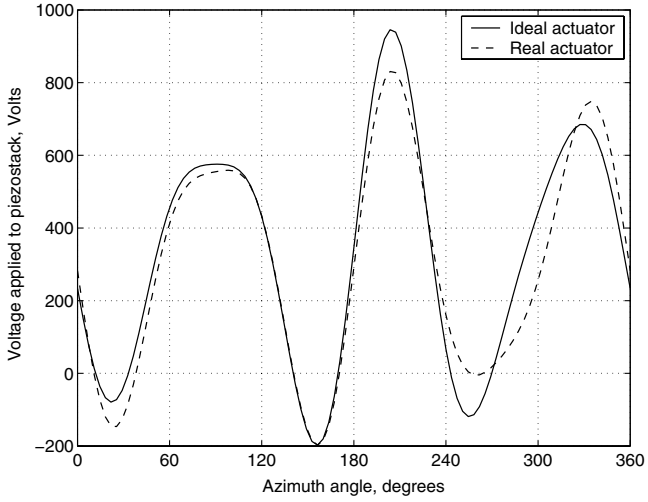


**Fig. 14 Optimal multicyclic control input, $\mu = 0.30$.**

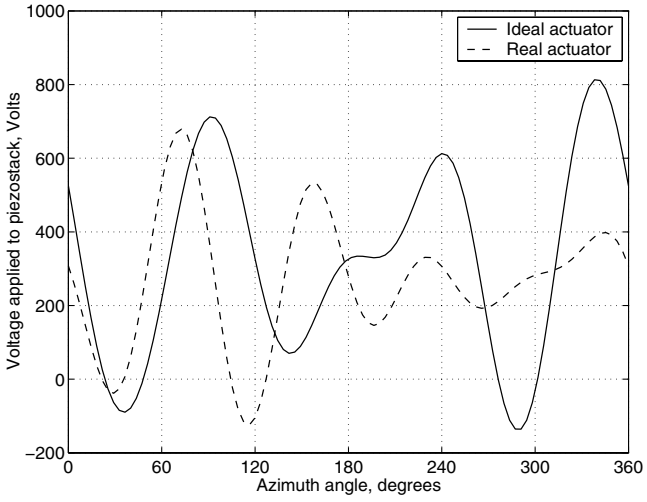


**Fig. 17 Optimal multicyclic control input, $\mu = 0.15$.**

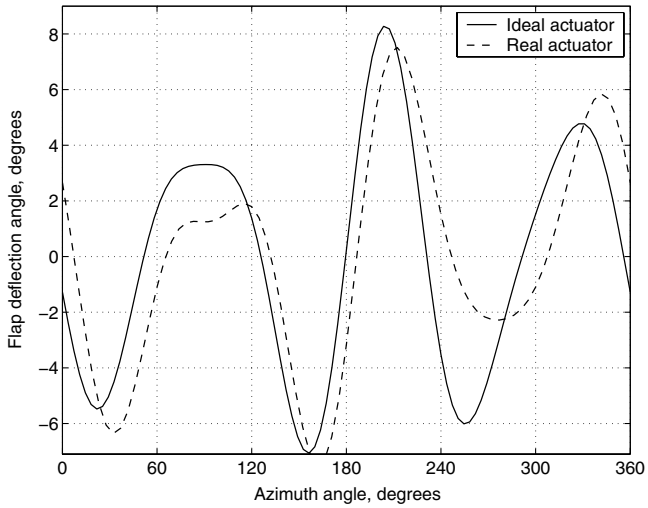


**Fig. 15 Flap motion history due to multicyclic control input, $\mu = 0.30$.**

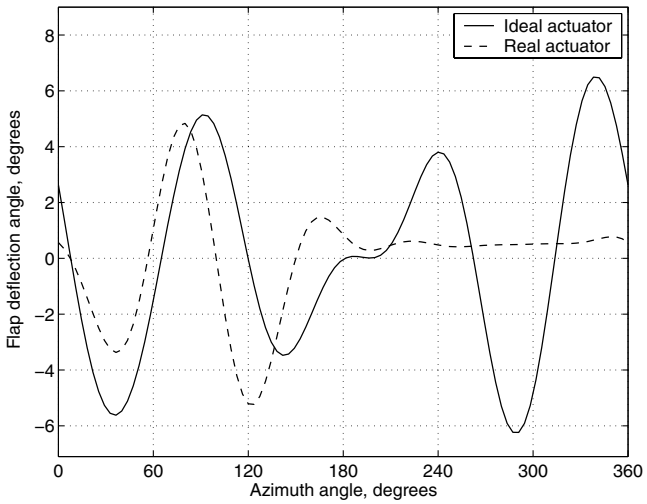


**Fig. 18 Flap motion history due to multicyclic control input, $\mu = 0.15$.**

Figure 14 shows the optimal control input for the two cases. Note that the optimal control input which needs to be given to the piezostack is different for the real actuator compared to the ideal actuator. However, in both cases, the actuators are used to complete authority in contrast to the single frequency control input cases. Unlike single frequency control input, the optimal flap motion history for the multicyclic control input is different for the two cases (see Fig. 15). Hub vibration is reduced by 90% and 81% from the baseline value for

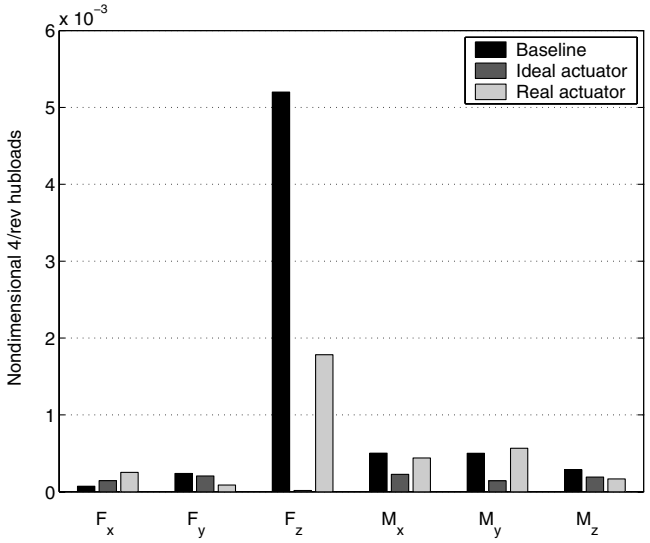


**Fig. 19 Comparison of hub vibratory loads for multicyclic control input, $\mu = 0.15$.**

the ideal and real actuator, respectively. This is because, for the real actuator, the system response is fairly nonlinear with respect to multicyclic control input. This shows that neglecting hysteresis in the actuator leads to overprediction in vibration reduction compared to an actuator with hysteresis modeled. Figure 16 shows the reduction in the individual vibratory hubloads.

Figures 6, 10, and 12 indicate that the actuator is not used to its full potential when the optimal control input is given at a single frequency. That is, the constraints on the minimum and maximum voltage that could be applied to the piezostack actuator (from Fig. 5) are not active at the optima. However, in the case of multicyclic input, the actuator is used to its full potential (Fig. 14).

#### Vibration Reduction at Low-Speed Flight ($\mu = 0.15$)

The results shown in the preceding section were obtained at a high forward speed corresponding to an advance ratio of 0.30. Studies are also performed at a low forward speed of advance ratio 0.15. For the ideal actuator, overall vibration reduction of 90, 98, and 91% is achieved by using 3/rev, 4/rev, and 5/rev control input, respectively. For the real actuator, hub vibration is reduced by 88, 84, and 91% from baseline level through 3/rev, 4/rev, and 5/rev control input, respectively. Multicyclic control input gave 99 and 86% reduction in hub vibration for the ideal and real actuator, respectively. This indicates that not modeling hysteresis leads to results showing much larger reduction in vibration compared with when hysteresis is modeled. Figure 17 shows the optimal multicyclic control input obtained for the two cases. The flap motion for the two cases are quite different (Fig. 18). The reductions in individual hub vibratory loads are given in Fig. 19. It is clear that the ideal linear actuator performs better than the real actuator with hysteresis modeled.

Table 2 summarizes the numerical results obtained in terms of hub vibration reduction for the ideal and real actuator at high and low forward speeds. It should be noted that a static hysteresis model is used in this work as a first step into this research area.

## Conclusions

In this paper, the effect of actuator hysteresis on helicopter vibration control using a trailing-edge flap is studied. Two cases are considered: 1) ideal linear actuator and 2) real actuator with hysteresis nonlinearity. The global controller is used to determine the optimal control input for the ideal linear actuator. The feedback form of the global controller is used in the case of the real actuator with hysteresis. This controller is known to work well in systems with weak nonlinearity. The controller performance is compared for two cases. The hysteresis in the real actuator is modeled using the classical Preisach model. The weighting function which is characteristic of the hysteresis transducer is estimated from experimental data found in literature. Active vibration control is simulated for steady-state high and low forward speed conditions. The following conclusions can be drawn from the results presented in this paper for a four-bladed hingeless rotor similar to the BO105 rotor:

In high-speed flight, both ideal linear actuator and real actuator give 79, 70, and 66% reduction in hub vibration using individual 3/rev, 4/rev, and 5/rev control inputs, respectively. In the case of real actuator, the addition of actuator hysteresis made the overall system more nonlinear. Therefore, the voltage control input required for obtaining minimum vibration levels is different in the two cases. However, the resulting flap motion in the two cases are almost identical for single frequency control inputs.

The ideal linear actuator with multicyclic control input gives 90% reduction in hub vibration at high-speed flight. The real actuator with multicyclic control input resulted in only 81% in hub vibration reduction. This loss in controller performance (about 9%) in the real actuator is due to the presence of actuator hysteresis. Again, the optimal voltage control input for the two cases are different. However, unlike single frequency control input, the resulting flap motion due to multicyclic control input in the two cases are not identical.

For an ideal linear actuator in low-speed flight, vibration levels are reduced by 90, 98, 91, and 99% with 3, 4, 5/rev, and multicyclic control input, respectively. For 3/rev and 5/rev control input, the performance of the real actuator is comparable to the ideal linear actuator. However, for 4/rev and multicyclic control input the real actuator yielded only 84 and 86% reduction in vibration levels, respectively. Again this performance penalty (a drop of 14%) can be attributed to the presence of hysteretic nonlinearity in the flap actuator.

In the case of multicyclic control input, both ideal and real actuators are used over the complete envelope of authority in high-speed flight. However, in low-speed flight, the actuators are not required to operate over their complete envelope of authority to achieve maximum vibration suppression.

The incorporation of more complex and accurate hysteresis models like dynamic hysteresis models can strengthen the nonlinearity and further penalize the controller performance. This is a subject of future work.

**Table 2 Percentage reduction in hub vibration for all cases**

| Type of control input | Ideal linear actuator | Real actuator with hysteresis | Ideal linear actuator | Real actuator with hysteresis |
|---|---|---|---|---|
| | High-speed flight ($\mu = 0.30$) | | Low-speed flight ($\mu = 0.15$) | |
| 3/rev | 79 | 79 | 90 | 88 |
| 4/rev | 70 | 70 | 98 | 84 |
| 5/rev | 66 | 66 | 91 | 91 |
| Multicyclic | 90 | 81 | 99 | 86 |

## References


[1] Nguyen, K., and Chopra, I., "Application of Higher Harmonic Control to Rotor Operating at High Speed and Thrust," *Journal of the American Helicopter Society*, Vol. 35, No. 3, 1990, pp. 78–89.

[2] Wood, R., Powers, R., Cline, J., and Hammond, C., "On Developing and Flight Testing a Higher Harmonic Control System," *Journal of the American Helicopter Society*, Vol. 30, No. 1, 1985, pp. 3–20.

[3] Friedmann, P. P., and Millott, T. A., "Vibration Reduction in Rotorcraft Using Active Control: A Comparison of Various Approaches," *Journal of Guidance, Control, and Dynamics*, Vol. 18, No. 4, 1995, pp. 664–673.

[4] Kunze, O., Arnold, U. T. P., and Waaske, S., "Development and Design of an Individual Blade Control System for the Sikorsky CH-53G Helicopter," *Proceedings of the 55th Annual Forum of the American Helicopter Society*, AHS International, Alexandria, VA, 1999, pp. 2272–2281.

[5] Wilbur, M., Mirick, P., Yeager, W., Langston, C., Cesnik, C., and Shin, S., "Vibratory Loads Reduction Testing of the NASA/Army/MIT Active Twist Rotor," *Journal of the American Helicopter Society*, Vol. 47, No. 2, 2002, pp. 123–133.

[6] Friedmann, P., de Terlizzi, M., and Myrtle, T., "New Developments in Vibration Reduction with Actively Controlled Trailing Edge Flaps," *Mathematical and Computer Modelling*, Vol. 33, Nos. 10–11, May–June 2001, pp. 1055–1083.

[7] Fulton, M., and Ormiston, R., "Hover Testing of a Small Scale Rotor with On-Blade Elevons," *Journal of the American Helicopter Society*, Vol. 46, No. 2, 2001, pp. 96–106.

[8] Koratkar, N., and Chopra, I., "Closed-Loop Wind Tunnel Testing of a Smart Rotor Model with Trailing-Edge Flaps," *Journal of the American Helicopter Society*, Vol. 47, No. 4, 2002, pp. 263–272.

[9] Ormiston, R., "Aeroelastic Considerations for Rotorcraft Primary Control with On-Blade Elevons," *Proceedings of the 57th Annual Forum of the American Helicopter Society*, AHS International, Alexandria, VA, 2001, pp. 1033–1049.

[10] Milgram, J., and Chopra, I., "A Parametric Design Study for Actively Controlled Trailing Edge Flaps," *Journal of the American Helicopter Society*, Vol. 43, No. 2, 1998, pp. 110–119.

[11] Milgram, J., Chopra, I., and Straub, F., "Rotors with Trailing Edge Flaps: Analysis and Comparison with Experimental Data," *Journal of the American Helicopter Society*, Vol. 43, No. 4, 1998, pp. 319–332.

[12] Straub, F., and Charles, B., "Aeroelastic Analysis of Rotors with Trailing Edge Flaps Using Comprehensive Codes," *Journal of the American Helicopter Society*, Vol. 46, No. 3, 2001, pp. 192–199.

[13] de Terlizzi, M. D., and Friedmann, P. P., "Active Control of BVI Induced Vibrations Using a Refined Aerodynamic Model and Experimental Correlation," *Proceedings of the 55th Annual Forum of the American Helicopter Society*, AHS International, Alexandria, VA, 1999, pp. 599–618.

[14] Liu, L., Patt, D., and Friedmann, P. P., "Simultaneous Vibration and Noise Reduction in Rotorcraft Using Aeroelastic Simulation," *Proceedings of the 60th Annual Forum of the American Helicopter Society*, AHS International, Alexandria, VA, 2004, pp. 1648–1672.

[15] Friedmann, P. P., "Vibration Reduction in Rotorcraft Using Actively Controlled Flaps—From Theoretical Concept to Flight Ready Hardware," *Proceedings of the Confederation of European Aerospace Societies/AIAA Joint International Forum on Structural Dynamics and Aeroelasticity*, Netherlands Association of Aeronautical Engineers, Amsterdam, 2003, pp. 1–22.

[16] Shen, J., and Chopra, I., "Swashplateless Helicopter Rotor with Trailing-Edge Flaps," *Journal of Aircraft*, Vol. 41, No. 2, 2004, pp. 208–214.

[17] Celi, R., "Stabilization of Helicopter Blades with Severed Pitch Links Using Trailing-Edge Flaps," *Journal of Guidance, Control, and Dynamics*, Vol. 26, No. 4, 2003, pp. 585–592.

[18] Zhang, J., Smith, E., and Wang, K., "Active-Passive Hybrid Optimization of Rotor Blades with Trailing Edge Flaps," *Journal of the American Helicopter Society*, Vol. 49, No. 1, 2004, pp. 54–65.

[19] Spencer, M., Sanner, R., and Chopra, I., "Adaptive Neurocontrol of Simulated Rotor Vibrations Using Trailing Edge Flaps," *Journal of Intelligent Material Systems and Structures*, Vol. 10, No. 11, 1999, pp. 855–871.

[20] Lee, T., and Chopra, I., "Design of Piezostack-Driven Trailing Edge Flap Actuator for Helicopter Rotors," *Smart Materials and Structures*, Vol. 10, No. 1, 2001, pp. 15–24.

[21] Hall, S. R., and Prechtl, E. F., "Preliminary Testing of a Mach-Scaled Active Rotor Blade with a Trailing Edge Servo-Flap," *Proceedings of SPIE Conference on Smart Structures and Materials*, International Society for Optical Engineering, Bellingham, WA, 1999, pp. 14–21.

[22] Kurdila, A. J., Li, J., Strganac, T., and Webb, G., "Nonlinear Control Methodologies for Hysteresis in PZT Actuated On-Blade Elevons," *Journal of Aerospace Engineering*, Vol. 16, No. 4, 2003, pp. 167–176.

[23] Leishman, J. G., and Beddoes, T. S., "A Semi-Empirical Model for Dynamic Stall," *Journal of the American Helicopter Society*, Vol. 34, No. 3, 1989, pp. 3–17.

[24] Hariharan, N., and Leishman, J. G., "Unsteady Aerodynamics of a Flapped Airfoil in Subsonic Flow by Indicial Concepts," *Journal of Aircraft*, Vol. 33, No. 5, 1996, pp. 855–868.

[25] Bagai, A., and Leishman, J. G., "Rotor Free-Wake Modeling Using a Pseudo-Implicit Technique Including Comparisons with Experimental Data," *Journal of the American Helicopter Society*, Vol. 40, No. 3, 1995, pp. 29–41.

[26] Viswamurthy, S. R., and Ganguli, R., "An Optimization Approach to Vibration Reduction in Helicopter Rotors with Multiple Active Trailing Edge Flaps," *Aerospace Science and Technology*, Vol. 8, No. 3, 2004, pp. 185–194.

[27] Leishman, J. G., "Inidicial Lift Approximations for Two-Dimensional Subsonic Flow as Obtained from Oscillatory Measurements," *Journal of Aircraft*, Vol. 30, No. 3, 1993, pp. 340–351.

[28] Gandhi, F., and Tauzig, L., "A Critical Evaluation of Various Approaches for the Numerical Detection of Helicopter Blade-Vortex Interactions," *Journal of the American Helicopter Society*, Vol. 45, No. 3, 2000, pp. 179–190.

[29] Preisach, F., "On Magnetic Aftereffect," *Zeitschrift für Physik*, Vol. 94, 1935, pp. 277–302.

[30] Sreeram, P. N., and Naganathan, N. G., "Hysteresis Prediction for a Piezoceramic Material System," *Proceedings of 1993 ASME Winter Annual Meeting*, ASME International, New York, 1993, pp. 35–42.

[31] Hughes, D., and Wen, J. T., "Preisach Modeling of Piezoceramic and Shape Memory Alloy Hysteresis," *Smart Materials and Structures*, Vol. 6, No. 3, 1997, pp. 287–300.

[32] Ge, P., and Jouaneh, M., "Modeling Hysteresis in Piezoceramic Actuators," *Precision Engineering*, Vol. 17, No. 3, 1995, pp. 211–221.

[33] Krasnoselskii, M. A., and Pokrovskii, A. V., *Systems with Hysteresis*, Springer–Verlag, New York, 1989, pp. 1–57.

[34] Mayergoyz, I. D., "On Numerical Implementation of Hysteresis Models," *IEEE Transactions on Magnetics*, Vol. 21, No. 5, 1985, pp. 1853–1855.

[35] Johnson, W., "Self-Tuning Regulators for Multicyclic Control of Helicopter Vibration," NASA Technical Paper 1996, March 1982.

[36] Millott, T. A., "Vibration Reduction in Helicopter Rotors Using an Active Controlled Partial Span Trailing Edge Flap Located on the Blade," Ph.D. Thesis, Univ. of California, Los Angeles, 1993.

[37] Millott, T. A., and Friedmann, P. P., "Vibration Reduction in Helicopters Rotors Using an Actively Controlled Partial Span Trailing Edge Flap Located on the Blade," NASA CR-4611, June 1994.